Effect of Helicity and Rotation on the Free Decay of Turbulent Flows

T. Teitelbaum[1] and P. D. Mininni[1,2]

[1]*Departamento de Física, Facultad de Ciencias Exactas y Naturales, Universidad de Buenos Aires and CONICET, Ciudad Universitaria, 1428 Buenos Aires, Argentina*

[2]*NCAR, P.O. Box 3000, Boulder, Colorado 80307-3000, USA*

(Received 26 November 2008; published 29 June 2009)

The self-similar decay of energy in a turbulent flow is studied in direct numerical simulations with and without rotation. Two initial conditions are considered: one nonhelical (mirror symmetric) and one with maximal helicity. While in the absence of rotation the energy in the helical and nonhelical cases decays with the same rate, in rotating flows the helicity content has a major impact on the decay rate. These differences are associated with differences in the energy and helicity cascades when rotation is present. The properties of the structures in the flow at late times are also discussed.

DOI: 10.1103/PhysRevLett.103.014501 PACS numbers: 47.27.ek, 47.27.Ak, 47.27.Jv, 47.32.Ff

Turbulence is ubiquitous in nature, and many turbulent flows are also rotating. The effect of rotation becomes important when the Rossby (Ro) number (the ratio of the convective to the Coriolis acceleration) is sufficiently small. Midlatitude synoptic scales in the atmosphere, stellar convective regions, and turbo machinery are examples of such flows. Helicity (alignment of the velocity and the vorticity) is also important for many processes in astrophysical, geophysical, and engineering flows. As an example, helical flows were proposed as the reason for the stability of rotating convective thunderstorms [1].

Studies of helical homogeneous and isotropic turbulence (HIT) [2,3] showed that the helicity and the energy are transferred toward smaller scales with constant fluxes. Moreover, it was observed that the energy scaling (Kolmogorov's law) was unchanged by helicity. As a result, helicity is expected to globally arrest the energy decay, but not to change its self-similar decay rate. Nonhelical rotating turbulence (RT) has been studied in detail [4], but because of the similarities between the helical and nonhelical cases in HIT, not much attention has been paid to helicity in the rotating case.

The lack of detailed studies of helical RT is remarkable considering the relevance of helicity and rotation in many astrophysical and geophysical processes. In this work, we study the effect of rotation and of helicity upon the self-similar decay of energy in turbulent flows. Even in HIT, the law for the decay rate of energy is a matter of debate [5]. It is known that it depends on properties of the infrared energy spectrum (i.e., the spectrum at scales larger than the energy-containing scale), and may depend on other statistical properties of the initial conditions. As a result, in this Letter we will consider only two flows with the same infrared spectrum and the same energy decay rate in the absence of rotation, and study how the presence of helicity and rotation changes their decay. A different decay is found for helical RT in numerical simulations. The results are interpreted in terms of how the energy and helicity cascades are modified by rotation, and a phenomenological theory is discussed.

The numerical simulations solve the Navier-Stokes equations for an incompressible fluid in a rotating frame,

$$\partial_t \mathbf{u} + \boldsymbol{\omega} \times \mathbf{u} + 2\boldsymbol{\Omega} \times \mathbf{u} = -\boldsymbol{\nabla}\mathcal{P} + \nu \boldsymbol{\nabla}^2 \mathbf{u}, \qquad (1)$$

where $\mathbf{u}$ is the velocity field ($\boldsymbol{\nabla} \cdot \mathbf{u} = 0$), $\boldsymbol{\omega} = \boldsymbol{\nabla} \times \mathbf{u}$ is the vorticity, $\mathcal{P}$ is the total pressure (modified by the centrifugal term), and ν is the kinematic viscosity. We chose the rotation axis to be in the z direction, $\boldsymbol{\Omega} = \Omega \hat{z}$, with Ω the rotation frequency. Our integration domain is a periodic box of length 2π. Two sets of runs were done at resolutions of 256^3 (set A) and 512^3 grid points (set B) using a dealiased pseudospectral code (see Table I).

To simulate systems with different amounts of initial relative helicity ($h = H/\langle|\mathbf{u}||\boldsymbol{\omega}|\rangle$, where $H = \langle \mathbf{u} \cdot \boldsymbol{\omega} \rangle$ is the flow net helicity), two flows were considered as initial conditions: the Taylor-Green (TG) flow [6] and the Arnold-Beltrami-Childress (ABC) flow [7]. The TG flow is nonhelical, and has zero energy in the $k_z = 0$ modes, whose amplification observed in the rotating cases (see below) is thus only due to a cascade process. The TG flow was chosen for its importance in hydrodynamics; it was originally motivated as an initial condition which leads to rapid development of small spatial scales. It also mimics the

TABLE I. Parameters used in the simulations: kinematic viscosity ν, rotation rate Ω, Reynolds number (Re), Rossby number (Ro), micro-Rossby number (Ro^ω), Ekman number E_k, initial relative helicity h, and at the time of maximum dissipation t^* (h^*). The values of Re, Ro, Ro^ω, and E_k are given at t^*.

Run	ν	Ω	Re	Ro	Ro^ω	E_k	h	h^*
A1	1.5×10^{-3}	0	450	⋯	⋯	⋯	0	0
A2	1.5×10^{-3}	0	600	⋯	⋯	⋯	0.95	0.34
A3	1.5×10^{-3}	4	550	0.12	1.28	2.2×10^{-4}	0	0
A4	1.5×10^{-3}	4	830	0.083	0.8	1.0×10^{-4}	0.95	0.65
B1	7×10^{-4}	4	1100	0.12	1.82	1.1×10^{-4}	0	0
B2	7×10^{-4}	4	1750	0.083	1.15	4.7×10^{-5}	0.95	0.44

von Kármán flows between two counterrotating disks used in several experiments. The ABC flow is an eigenfunction of the curl operator and as a result has maximum helicity. It was used as a paradigmatic example to study helical flows in the atmosphere [1]. Both flows develop, after a short time, an infrared energy spectrum proportional to k^2; this is important to ensure we can compare the decay rates of both flows.

The simulations were started using a superposition of these flows from wave numbers $k = 4$–14 with initial energy spectrum $\sim k^{-4}$. Runs with zero relative helicity have a superposition of TG flows, and runs with $h \approx 0.95$ have a superposition of ABC flows. The runs were extended for over 40 turnover times, and the dissipative range was properly resolved with the ratio $k_\eta/k_{\max} < 0.85$ at all times, where k_η is the dissipation wave number and $k_{\max}$ the maximum resolved wave number. Times in the figures are expressed in units of the turnover time at $t = 0$, $T = L/U$, where $L \approx 2\pi/k_0 = 2\pi/4$ and $U \approx 1$ are the initial integral scale and rms velocity.

Several Reynolds (Re), Rossby, and Ekman numbers can be defined for the runs. We will consider here the Reynolds number based on the integral scale $\mathrm{Re} = UL/\nu$, and the accompanying Rossby number $\mathrm{Ro} = U/(2\Omega L)$. The integral scale is defined as $L = 2\pi \int E(k)k^{-1}dk/E$, where $E(k)$ is the isotropic energy spectrum and E is the total energy. The Ekman number is then defined as $E_k = \mathrm{Ro}/\mathrm{Re}$. At $t = 0$ runs in set A have $\mathrm{Re} \approx 1050$ and runs in set B have $\mathrm{Re} \approx 2250$. At the same time the Rossby number is $\mathrm{Ro} \approx 0.08$ for runs A3, A4, and B1-B2; the initial Ekman number is then $E_k \approx 7.6 \times 10^{-5}$ in runs A3 and A4, and $E_k \approx 3.6 \times 10^{-5}$ in runs B1-B2. Values of the controlling parameters for each run at the time of maximum dissipation t^* are given in Table I.

It is also convenient to introduce a microscale Rossby number as $\mathrm{Ro}^\omega = \omega/(2\Omega)$ [8]. It can be interpreted as the ratio of the convective to the Coriolis acceleration at the Taylor scale, a scale characteristic of the turbulent inertial range. In order for anisotropies to develop in the simulations, the Rossby number must be small enough for the rotation to affect the turbulence, but the micro-Rossby Ro^ω must be larger than one for scrambling effects of inertial waves not to completely damp the nonlinear terms (which leads to a pure exponential viscous decay) [9]. We are interested in simulations with moderate rotation rates to ensure $\mathrm{Ro} \lesssim 1$ and with Re large enough to have enough scale separation between the energy-containing and the dissipative scale. Note in Table I how Ro and Ro^ω are 1 order of magnitude apart in all runs at time t^*. This difference is sustained in time during the self-similar energy decay.

Figure 1 shows the time history of the energy and enstrophy in runs A1, A2, B1-B2. In all runs there is a self-similar decay after the time t^*. Runs A3 and A4 (not shown) decay, respectively, as runs B1 and B2, although the time span of the self-similar stage is shorter. In both runs with $\Omega = 0$, the energy decays as $\sim t^{-2}$. As will be discussed later, this exponent corresponds to the decay of a flow with constant integral length [10].

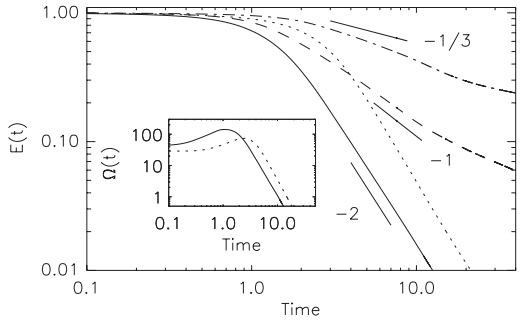

FIG. 1. Energy evolution for runs A1 (solid curve), A2 (dotted curve), B1 (dashed curve), and B2 (dot-dashed curve). Runs A1 and A2 have $\Omega = 0$ and decay with the same rate independently of the helicity content. When rotation is turned on the decay rates differ. Inset: Enstrophy evolution for runs A1 and A2.

Helicity in run A2 does not seem to affect the self-similar decay, as predicted in [3]. This is in good agreement with the fact that helicity does not change the spectral index of the energy in HIT [2]. However, the self-similar decay in run A2 starts at a later time, as previously reported in Ref. [11]. This is associated with the slowdown in the generation of small scales in helical flows [12], which results in a longer time to reach the maximum of dissipation in run A2 (see the inset of Fig. 1).

In runs with rotation (A3, A4, B1, and B2), a transient is also observed before t^*. Then, self-similar decays with different power laws for the energy are found in all runs. Runs A3 and B1 have a decay near t^{-1} [13,14], while the runs with maximum helicity (A4 and B2) follow a decay slightly faster than $t^{-1/3}$. Contrary to HIT, we can appreciate now how helicity truly affects the self-similar decay. As will be shown later, in RT the energy decays between t^{-1} and $t^{-1/3}$, with t^{-1} corresponding to nonhelical RT and $t^{-1/3}$ to maximally helical RT, a case difficult to obtain in the simulations.

The time evolution is accompanied by a change in the energy spectrum; see Fig. 2(a). While the runs without rotation show at t^* and during the self-similar decay a spectrum consistent with Kolmogorov scaling in both the energy and the helicity, runs with rotation show different slopes. Run B1 (which has a larger scale separation than run A3) shows for $t \geq t^*$ an isotropic energy spectrum compatible with k^{-2} (the anisotropic spectrum is also compatible with $\sim k_\perp^{-2}$) [15,16]. The energy spectrum in run B2 is slightly steeper than in run B1, while the helicity spectrum is shallower than the energy spectrum. The product of both spectra is consistent with a k^{-4} law, as predicted using phenomenology in [16]. Indeed, the spectrum of relative helicity measured in B2 is $\sim k^{-0.6}$, while in helical HIT the relative helicity scales as k^{-1}. As a result, there is an excess of helicity on the small scales in run B2, which results in quenching of nonlinearities and a further reduced energy dissipation rate and decay. It is worth mentioning

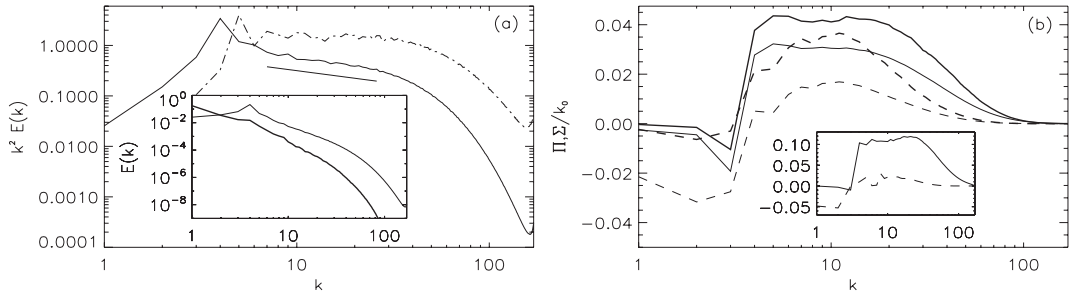

FIG. 2. (a) Isotropic energy spectrum compensated by k^{-2} for runs B1 (dot-dashed curve) and B2 (solid curve) near the peak of dissipation. The helical flow shows a steeper spectrum. A $k^{-2.5}$ slope (corresponding to $k^{-1/2}$ in the compensated plot) is shown as a reference). Inset: Isotropic energy spectrum for run B2 at $t \approx 8$ (thin curve) and $t \approx 30$ (thick curve). (b) Energy flux $\Pi(k)$ (thin curve) and helicity flux $\Sigma(k)$ (thick curve) across scales, for run B2 at $t \approx 5$ (solid curve) and $t \approx 13$ (dashed curve); $\Sigma(k)$ is normalized by the initial energy-containing wave number $k_0 \approx 4$. Inset: Energy flux $\Pi(k)$ for run B1 at $t \approx 2$ (solid curve) and $t \approx 11$ (dashed curve). Positive flux indicates a direct cascade, and negative flux indicates an inverse cascade.

that spectral slopes are better measured in forced runs, where a turbulent steady state can be reached (see [16]). However, as can be seen from Fig. 2(a), near the peak of dissipation the spectra of runs B1 and B2 clearly differ. Note t^* is the time when turbulence fully develops and the largest scale separation is attained. During the subsequent self-similar decay, the slopes do not change significantly.

In the runs with rotation, a change in the small-scale spectrum is observed at $t \approx 20$. As energy piles up at the largest available scale in the box and columnlike structures form in the velocity, the small-scale energy spectrum becomes steeper. This is accompanied by a decrease in the decay rate of the energy (see Fig. 1). This process is reminiscent of the change observed in the free decay of two-dimensional turbulence, when the coalescence of large-scale vortices at late times leads to a steeper energy spectrum and a change in the self-similar decay [17].

Runs A1 and A2 develop direct energy fluxes toward small scales while the rotating nonhelical runs (A3 and B1) show both a direct and an inverse energy cascade [see the inset of Fig. 2(b)]. In the helical runs [Fig. 2(b)], at $t \approx 2$ we observe maximum positive flux of energy and helicity toward smaller scales, evidencing both energy and helicity having a direct cascade. However, the helicity flux is larger than the direct energy flux. Later, an inverse cascade of energy can be clearly identified from the negative energy flux at large scales. At $t \approx 13$, the coexistence of both an inverse cascade of energy and direct cascades of energy and helicity is observed.

Although Figs. 2(a) and 2(b) show the isotropic spectras and fluxes, the flows in the rotating case are anisotropic. Most of the energy in the spectra is in modes perpendicular to the axis of rotation, and the anisotropic spectrum $E(k_\perp)$ and flux $\Pi(k_\perp)$ look similar to the ones previously discussed. We present instead some global indications of the development of anisotropies. Figure 3 shows the ratio of the energy in perpendicular modes (i.e., modes with $k_z = 0$) to the total energy in runs B1 and B2. Differences at early times are due to different initial conditions. However, it can be seen that both curves grow monotonically to a value near 1, indicating that the flows evolve toward anisotropic states as the energy is transferred to perpendicular modes [4]. A measure of small-scale anisotropy is given by the Shebalin angle

$$\tan^2\theta = 2\frac{\sum_{k=1}^{k_{\max}} k_\perp^2 E(k_\perp)}{\sum_{k=1}^{k_{\max}} k_\parallel^2 E(k_\parallel)}. \quad (2)$$

Its evolution in runs B1 and B2 can be seen in the inset of Fig. 3. It grows monotonically although in run B2 it reaches a maximum at $t \approx 12$ and then seems to saturate. A similar behavior is observed for $L_\parallel$ (not shown) which again grows monotonically in B1 but reaches a maximum in B2 at approximately the same time. In all cases, $\tan^2\theta \gg 2$, which corresponds to anisotropic flows.

The increase of the correlation lengths, together with the growth of $E(k_z = 0)/E$ and of $\tan^2\theta$, speaks of anisotropization of the flows. This tendency towards two-dimensionalization is confirmed by exploring the flows in real space. Figure 4 shows visualizations of the rms vorticity with superimposed velocity field lines for runs A3 and A4 at late times ($t \approx 45$). In both cases, a strong anisotropy is observed with large-scale columnlike struc-

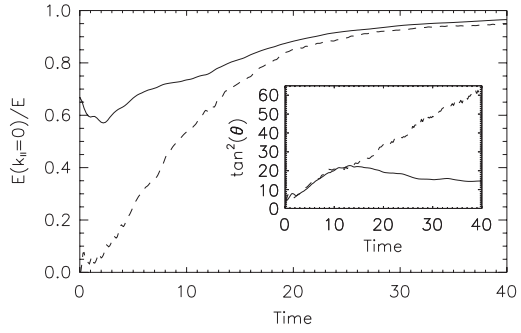

FIG. 3. Ratio of the energy in modes with $k_\parallel = 0$ to the total energy in runs B1 (dashed curve) and B2 (solid curve). Despite the different initial conditions, the curves grow monotonically to 1, showing a transfer of energy to perpendicular modes. Inset: Time evolution of the Shebalin angle for the same runs.

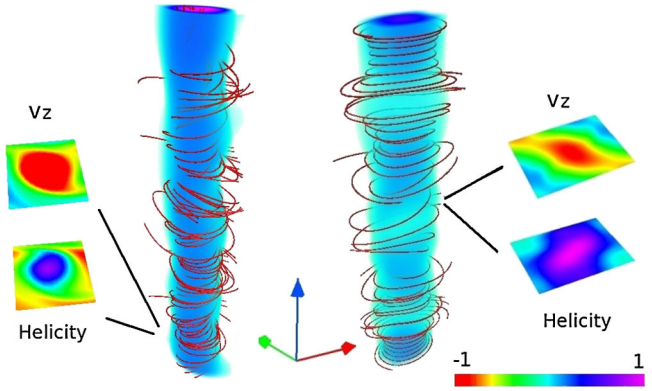

FIG. 4 (color online). Visualizations of the rms vorticity for $t \approx 45$ with superimposed velocity field lines for runs A3 (right) and A4 (left). Cuts of v_z and H on a plane perpendicular to $\mathbf{\Omega}$ are shown. The color table gives the amplitudes normalized to the maximum of each quantity.

tures in the vorticity (similar structures are observed if energy density is visualized instead). However, a significant difference in the geometry of the flow in the columns is observed between runs A3 and A4 . While the flow in the columns of the helical run is strongly helical (the flow goes either up or down in the entire column, thus giving helical velocity field lines), the columns of the nonhelical run have no net helicity (the flow goes up and down inside the same column). This indicates that even at late times the properties of the emerging structures in rotating flows depend on the initial helicity content.

The distinct evolution in the free decay of helical and nonhelical flows when rotation is present can be understood in terms of a simple phenomenological theory. For HIT we make use of the classical Kolmogorov phenomenology which leads to the well-known energy spectrum $E(k) \sim \epsilon^{2/3} k^{-5/3}$, where ϵ represents the energy dissipation rate. From the Navier-Stokes equation it is easy to show that for a freely decaying flow $dE/dt \sim E^{3/2}/L$, which leads to a self-similar decay law $E(t) \sim t^{-2}$ if the integral scale is assumed constant [5,10].

In nonhelical RT, it is often assumed that $E(k) \sim \epsilon^{1/2} \Omega^{1/2} k^{-2}$ (we use the isotropic wave number k, although the arguments can be generalized to the anisotropic case replacing k by $k_\perp$). This spectrum was observed in 512^3 simulations of forced flows [15], obtained from closures [14], and derived from phenomenological arguments assuming the inertial waves slow down the energy cascade [18]. Using this spectrum it follows that $dE/dt \sim (E/L)^2$ resulting in a decay $E(t) \sim t^{-1}$ (the assumption of constant L is justified since k_0 in the initial conditions is close to the minimum wave number $k_{\min} = 1$; see [13]). This decay is consistent with experiments and simulations at lower resolution [11,13,14].

The case of helical RT differs from the previous two. In this case, the direct transfer is dominated by the helicity cascade. Writing the helicity flux as $\delta \sim h_l/(\Omega \tau_l^2)$, where h_l is the helicity at the scale l and τ_l the eddie turnover time, leads to a spectra $E(k) \sim k^{-n}$ and $H(k) \sim k^{n-4}$, where $n = 5/2$ for the case of maximum helicity [16]. Using $E(t) \sim \epsilon^\alpha \Omega^\beta k^{-5/2}$, dimensional analysis leads to $E(k) \sim \epsilon^{1/4} \Omega^{5/4} k^{-5/2}$ (see [16] also for forced runs). From $dE/dt \sim \epsilon/L$, then $dE/dt \sim E^4/L^{11}$, which for constant L leads to $E(t) \sim t^{-1/3}$ (note that for rotating flows with initial helicity between zero and the maximum, the decay rate is between -1 and $-1/3$; a run with relative helicity $h \approx 0.4$ was done to verify this).

The differences between HIT and RT when helicity is present open new directions in the study of rotating flows (the development of new subgrid models that take into account these differences being an example). This can also be the starting point to elucidate the role helicity plays in the decay of rotating flows in nature [1].

Computer time provided by NCAR and CECAR. P. D. M acknowledges support from Grant No. UBACYT X468/08.

[1] D. K. Lilly, Atmos. Sci. Rep. **43**, 126 (1986).
[2] O. G. Chkhetiani, JETP Lett. **63**, 808 (1996); V. Borue and S. A. Orszag, Phys. Rev. E **55**, 7005 (1997); Q. Chen, S. Chen, and G. L. Eyink, Phys. Fluids **15**, 361 (2003); P. D. Mininni, A. Alexakis, and A. Pouquet, Phys. Rev. E **74**, 016303 (2006).
[3] R. H. Kraichnan, J. Fluid Mech. **59**, 745 (1973).
[4] C. Cambon and L. Jacquin, J. Fluid Mech. **202**, 295 (1989); F. Waleffe, Phys. Fluids A **5**, 677 (1993); C. Cambon, N. N. Mansour, and F. S. Godeferd, J. Fluid Mech. **337**, 303 (1997).
[5] P. G. Saffman, Phys. Fluids **10**, 1349 (1967); U. Frisch, *Turbulence: The Legacy of A. N. Kolmogorov* (Cambridge University Press, Cambridge, England, 1995); L. Skrbek and S. R. Stalp, Phys. Fluids **12**, 1997 (2000); P. A. Davidson, *Turbulence* (Oxford University, New York, 2004).
[6] G. I. Taylor and A. E. Green, Proc. R. Soc. A **158**, 499 (1937).
[7] S. Childress and A. D. Gilbert, *Stretch, Twist, Fold: The Fast Dynamo* (Springer-Verlag, Berlin, 1995).
[8] L. Jacquin *et al.*, J. Fluid Mech. **220**, 1 (1990).
[9] C. Cambon, N. N. Mansour, and F. S. Godeferd, J. Fluid Mech. **337**, 303 (1997).
[10] L. Biferale *et al.*, Phys. Fluids **15**, 2105 (2003).
[11] Y. Morinishi, K. Nakabayashi, and S. Ren, JSME Int. J., Ser. B **44**, 410 (2001).
[12] J. C. André and M. Lesieur, J. Fluid Mech. **81**, 187 (1977).
[13] P. A. Davidson, P. J. Staplehurst, and S. B. Dalziel, J. Fluid Mech. **557**, 135 (2006); C. Morize and F. Moisy, Phys. Fluids **18**, 065107 (2006).
[14] F. Bellet *et al.*, J. Fluid Mech. **562**, 83 (2006).
[15] W. C. Müller and M. Thiele, Europhys. Lett. **77**, 34 003 (2007); P. D. Mininni, A. Alexakis, and A. Pouquet, Phys. Fluids **21**, 015108 (2009).
[16] P. D. Mininni and A. Pouquet, Phys. Rev. E **79**, 026304 (2009).
[17] J. C. McWilliams, J. Fluid Mech. **146**, 21 (1984).
[18] O. Zeman, Phys. Fluids **6**, 3221 (1994); Y. Zhou, Phys. Fluids **7**, 2092 (1995).